https://doi.org/10.5194/egusphere-2025-5086
Preprint. Discussion started: 26 January 2026

Optimization of the Gaussian Dispersion Model Inversion for Estimating Facility Scale Methane Emissions in Canada

Shoma Yamanouchi[1], Sebastien Ars[1], Meghan Flood[1], Lawson Gillespie[1], Jordan Stuart[1], Kiran Ramlogan[1], and Felix Vogel[1]

[1]Environment and Climate Change Canada: 4905 Dufferin St, North York, ON M3H 5T4, Canada

Correspondence: Shoma Yamanouchi (shoma.yamanouchi@ec.gc.ca)

Abstract. This study presents improvements to the implementation of Gaussian dispersion model for estimating methane (CH_4) emissions using mobile real-time measurements at facility scale. The Gaussian plume models often rely on discretized atmospheric states, characterized by stability classes. The proposed enhancements include blending (weighted averaging) the two nearest atmospheric stability classes to create a more continuous model of the atmosphere, and then systematically adjusting the source location along the transect to improve the fit. Stability classes (and the weights assigned) were derived by comparing surface roughness and Obukhov length. The source translation was performed by examining the shapes of the observed and modeled plume. The methods were tested on a widely used, open-source Gaussian dispersion model from Polyphemus, with mobile observations and a Bayesian inversion scheme to estimate emissions. Observations included both controlled release studies that were performed in Canada, as well as observation data from Canadian refineries and waste management facilities. A wide range of methane emission rates were examined, with estimating emissions ranging from 1.7 to 14,213 kg/day. Results showed that blending the stability classes results in model performance that are roughly the weighted averages of the two initial classes, and in some instances slightly better. Source translation resulted in increased correlation and decreased root mean square error (RMSE), in many cases significantly so (e.g., from R^2 of 0.02 to 0.96, seen in a transect from Courtright). The algorithm was also able to locate a previously unknown source. While blending stability classes showed small improvements in some cases, it generally aligned emission estimates with observations. Our novel approach worked across various stability classes, although its sensitivity to surface roughness remains a limitation for certain situations/environments.

1 Introduction

Understanding and quantifying the emissions of trace gases into the atmosphere is imperative for both air quality and climate change concerns. In fact, many nations have pledged to track and reduce their anthropogenic greenhouse gas (GHG) emissions in an effort to curb their impact on climate change following the recommendations made by the Intergovernmental Panel on Climate Change (IPCC, 2014). Canada, in particular, has committed to reduce its greenhouse gas emissions by 40 to 45%

https://doi.org/10.5194/egusphere-2025-5086
Preprint. Discussion started: 26 January 2026

below 2005 levels by 2030 and to achieve net zero emissions by 2050, with a strong emphasis on curbing methane emissions (see Government of Canada's Methane Strategy, available at https://www.canada.ca/en/services/environment/weather/climatechange/climate-plan/reducing-methane-emissions/faster-further-strategy.html; last accessed May 2025, for more details). Methane (CH_4) is the most significant anthropogenic GHG after carbon dioxide (CO_2), and has received much attention due to its potent radiative forcing effects. Indeed, the global warming potential (GWP), which measures how much heat a particular gas traps in the atmosphere relative to CO_2 (i.e., GWP of CO_2 is by definition 1) is 28 for methane over a 100-year time scale. Because methane has a shorter atmospheric lifetime compared to CO_2 (on the order of about 12 years compared to centuries-long persistence of CO_2) it has an immediate impact on global warming (Smith et al., 2021). This characteristic makes methane a critical target for mitigation strategies that aim to reduce the pace of climate change. The potential for rapid and noticeable changes from methane reduction efforts has led many to regard it as "low-hanging fruit" for emission control (e.g., Hansen et al., 2000; Christensen, 2018), and Canada in particular has explicitly stated in their methane strategy that targeting methane offers a cost-effective opportunity for Canada to make substantial near-term progress toward its climate goals. However, addressing methane emissions remains a significant challenge due to the complexities of accurately estimating its release into the atmosphere and identifying the specific sources of these emissions (e.g., Chang et al., 2019; Nisbet et al., 2020).

Quantifying methane emissions presents a difficult challenge due to a number of factors that contribute to uncertainty in emission estimates. There are two categories off approaches to estimating emissions. The first category is often referred to as "bottom-up" approaches. In bottom-up approaches, emissions are often calculated based on activity data and emission factors, or consumption-based statistics, all of which all of which have associated uncertainties. Furthermore, complex emissions models can incorporate factors such as meteorological conditions, terrain, and operational practices at emission sites can lead to significant variation in emission rates (Melton et al., 2013; Poulter et al., 2017). In contrast, top-down emission estimates, which rely on atmospheric measurements and often also employing inverse modeling techniques, offer a complementary approach by directly observing the concentrations of methane in the atmosphere. This approach also has uncertainties, both with the measurements and in the model used for the inversion, however it can provide an independent and direct estimate of emissions, and can also help identify localized hotspots of methane emissions. Revealing discrepancies between emission inventories and atmospheric-based estimates can provide valuable insights into emission process and inform targeted mitigation efforts. Studies such as Ars et al. (2020) have highlighted the importance of improving the identification of emission sources to reduce the uncertainties associated with methane estimates. In Canada, recent top-down studies have demonstrated that bottom-up inventories report may underestimate methane emissions from the oil and gas industry by between 25% and 90%. These discrepancies have been observed at various scales, from local facilities to national levels. Airborne studies have revealed significant discrepancies between reported and observed methane emissions from oil and gas production facilities, while mobile surveys in urban areas have highlighted the relevance of landfills and natural gas distribution infrastructure as methane sources (Johnson et al., 2017; Chan et al., 2020; Ars et al., 2020; MacKay et al., 2021; Tyner and Johnson, 2021). These findings underscore the importance of integrating top-down methods to enhance emission inventories and inform effec-

https://doi.org/10.5194/egusphere-2025-5086
Preprint. Discussion started: 26 January 2026

tive mitigation strategies.

At facility scale, one approach to top-down emissions estimates is to use a Bayesian inversion with Gaussian dispersion models. These models provide a relatively simple, computationally quick, and efficient method for calculating the distribution of pollutants, including methane, in the atmosphere. The use of Bayesian inversion for estimating CH_4 emissions have been well documented and well tested; it has been used with in-situ data(e.g., Ganesan et al., 2015; Bergamaschi et al., 2018; Yadav et al., 2019), satellite data (e.g., Alexe et al., 2015; Zhang et al., 2021; Cusworth et al., 2021), and aircraft data (e.g., Miller et al., 2013). Gaussian dispersion models work by calculating the spread of pollutants from a known source under specific meteorological conditions. The model gives a steady-state solution with constant emission rates as well as constant and homogeneous winds and terrain. By comparing the measured concentrations of methane at various locations with the predicted concentrations of the model, emissions from a particular source can be estimated. Although simplistic, this technique offers a valuable tool for modeling short-range transport and estimating emissions, as it is computationally less demanding than high-resolution atmospheric models that require extensive meteorological data and potentially significant computing resources.

Several studies (e.g., Hosseini and Stockie, 2016; Vogel et al., 2024; Gillespie et al., 2025) have demonstrated the use of Gaussian dispersion models in emission estimation, particularly in the context of urban or industrial sites. These models provide a practical way to assess emissions at multiple sites without the need for resource-intensive simulations. Despite their advantages, Gaussian models are not without limitations. For example, most Gaussian dispersion models use discretized atmospheric stability classes (Briggs, 1972), a parameter that affects the dispersion rate of pollutants. This parameter being discretized can result in systematic biases, depending on which class is chosen. Additionally, emissions calculated using this approach tend to be underestimated, with emission estimates being especially sensitive to the placement of the emitting source, which may not be well known (Ars et al., 2017). Many of the industrial sites that emit CH_4 are sized on the order of 100 m^2 to 1 km^2 and the emissions are typically emitted from several specific locations within the facilities, although the exact locations may not be identified exactly (Ars et al., 2017). Furthermore, as the model only describes the steady-state, with constant winds and emission rates, it may not fully capture the complex behaviors of trace gases under varying atmospheric conditions.

In this study, the Polyphemus gaussian dispersion model was used to estimate methane emissions, and to improve the performance of the model and inversion scheme, we present a novel method to blend stability classes in an attempt to represent a more continuous (i.e., less discretized) atmosphere, and an algorithm to adjust the source location parameter based on the statistics of posterior emission profiles and observations to obtain better emission estimates. The resulting model setup was tested on several landfills, waste treatment facilities, and oil refinement plants in Canada. Furthermore, in an attempt to reduce the effects of shifting winds, a method of sampling the same plume on the same road back to back and smoothing them to get an averaged plume was also tested. By integrating real-time trace gas measurements with Gaussian dispersion models and novel model optimization techniques, this study improves the robustness of methane emission estimates and offers valuable

https://doi.org/10.5194/egusphere-2025-5086
Preprint. Discussion started: 26 January 2026

insights for targeted mitigation strategies in various industrial contexts.

2 Methods

2.1 Mobile Measurements

The observational CH_4 data used for inversion in this study came from mobile measurements, where real-time data is collected from a vehicle-mounted sensor setup. The sampling inlet was mounted approximately 2.5 meters above ground to capture air samples at a height that would minimize interference from surface-level sources and ensure an accurate representation of ambient air concentrations (Vogel et al., 2024). The inlet was connected to a LI-7810 $CH_4/CO_2/H_2O$ OF-CEAS (Optical Feedback – Cavity Enhanced Absorption Spectroscopy) Trace Gas Analyzer manufactured by LI-COR Environmental (Lincoln, NE, USA). This instrument is capable of measuring CH_4 from 0 to 100 parts per million (ppm), with a precision of 0.60 parts per billion (ppb) at 2 ppm with 1 second averaging or 0.25 ppb at 2 ppm with 5 second averaging. The response time for these measurements is reported to be less than 2 seconds. Additionally, a weather station was also mounted on top of the vehicle to collect real-time meteorological data, including wind speed, wind direction, temperature, and atmospheric pressure (AIRMAR 220WX (Airmar Technology Corporation, Milford, NH, USA)).

2.2 Model Setup

To analyze the methane measurements collected from the mobile platform, and to run the inversion for estimating emissions, a Gaussian dispersion model from the Polyphemus suite (see Doi: 10.5281/zenodo.10067062 and https://cerea.enpc.fr/polyphemus/introduction.html; last accessed March, 2025) of atmospheric models was employed. The Polyphemus platform is supported by CEREA, Marne-la-Vallee, France, and is described in detail in Mallet et al. (2007). The Bayesian inversion process to estimate emissions was done following Ars et al. (2020). Bayesian inversion is particularly powerful because it integrates prior knowledge about emission sources and their characteristics with observed data, providing a probabilistic estimate of emission rates. Specifically, the posterior emissions were calculated as follows:

$$\mathbf{F_a} = \mathbf{F_b} + \mathbf{B}\mathbf{M}^{\mathrm{T}}(\mathbf{R}_{\mathrm{m}} + \mathbf{M}\mathbf{B}\mathbf{M}^{\mathrm{T}})^{-1}(\mathbf{Y} - \mathbf{M}\mathbf{F_b}), \tag{1}$$

and the uncertainty calculation as follows:

$$\mathbf{A} = (\mathbf{B}^{-1} + \mathbf{M}^{\mathrm{T}}\mathbf{R}_{\mathrm{m}}\mathbf{M})^{-1}, \tag{2}$$

where $\mathbf{F_a}$ and $\mathbf{F_b}$ are the posterior and prior methane emission rates, respectively, $\mathbf{A}$ and $\mathbf{B}$ are the uncertainties on the posterior and prior, respectively, $\mathbf{Y}$ is the observation, $\mathbf{M}$ is the observation operator, and $\mathbf{R}_{\mathrm{m}}$ is the covariance of the observation operator $\mathbf{M}$ (Tarantola, 2005). This method enables the incorporation of uncertainties in the input data and the model itself,

https://doi.org/10.5194/egusphere-2025-5086
Preprint. Discussion started: 26 January 2026

yielding more robust and reliable emission estimates. Emission sources were modeled to be 1-meter diameter circular area-sources for smaller sources (e.g., chimneys), and larger circles of up to 50-meters in diameter for larger area sources such as waste treatment ponds. Initial (a priori) estimates of emissions were taken to be 1 gram per second. Uncertainty analysis was performed based on the approach outlined by Ars et al. (2017). In their study, Ars et al. conducted several sensitivity tests on the Gaussian model to evaluate how each parameter impacts the emissions estimate. They found that the primary source of uncertainty was the selection of the stability class, accounting for 48 % of the uncertainty, followed by wind direction (38%), wind speed (28%), and source location (19%). They also found that parameters such as temperature, pressure, and measurement height were much smaller sources of uncertainty. The overall uncertainty of their method was estimated to be 75% of the final emissions estimate. In this study, the stability class and source location uncertainties were dropped, and the overall uncertainty was estimated to be 48% (the components added in quadrature).

Meteorological data from the High-Resolution Rapid Refresh (HRRRv4 native 3km resolution, see https://rapidrefresh.noaa.gov/hrrr/; last accessed March, 2025) reanalysis dataset (Dowell et al., 2022) provided by the National Oceanic and Atmospheric Administration (NOAA), USA, was used to drive the dispersion model. The HRRR data were chosen over the weather station data mounted on the vehicle due to the weather station having unreliable wind data when the vehicle was traveling at higher speeds, and because HRRR data is available across Canada. The HRRR dataset includes crucial parameters such as wind speed, wind direction, temperature, and planetary boundary layer (PBL) height, which are necessary for accurate predictions of gas dispersion. The PBL height defines the altitude at which the atmosphere becomes stably stratified, marking the boundary between the turbulent mixed layer and the free atmosphere. The mean of the latitude and longitude along the mobile measurement path was used to obtain the most representative coordinates for each transect. Most transects analyzed in this study were less than 3-km long.

2.2.1 Stability Classes

Gaussian dispersion models often rely on atmospheric stability classes, which provide a measure of how turbulent the atmosphere is, and directly affects the dispersion of pollutants. This parameter also affects plume-rise. In this study, a Briggs plume-rise scheme was used, which is a decision-tree-like algorithm that calculates the rise of a buoyant plume, with the stability class and buoyancy factor as inputs. The classes vary from A to F, A being extremely unstable, F being stable, and D being neutral. This was also derived from the HRRR data.

To improve the model, and in an attempt to get away from the discretized representation of the atmospheric processes, these classes were "blended" to better capture the continuous nature of the atmosphere. This was done following the relationship between surface roughness (z_0) and the inverse of the Obukhov length (L) (Golder curves) (Golder, 1972). They were used to compute a weighted average of the stability classes, allowing for a more continuous representation of the atmosphere. Specifically, the surface roughness and Obukhov length derived from HRRR were plugged into the Golder curves, and the position

https://doi.org/10.5194/egusphere-2025-5086
Preprint. Discussion started: 26 January 2026

in this z_0-$1/L$ plane and the distances to the nearest two classes were used to calculate the weighted average of the blended stability classes. The z_0-$1/L$ space and the curves on this plane are shown in Figure 1. For cases where the calculated position in the space was to the left of stability class A, or to the right of stability class F, then no blending was done. Blending was omitted if z_0 was extremely small ($z_0 < 0.002$) or large ($z_0 > 0.5$). These scenarios were not seen in any of the sites tested (although these conditions do appear in some extreme scenarios, such as in the middle of a city). Once the weights for the two stability classes were determined, the model was run as usual in these two modes, and the resulting fields were then blended by calculating the weighted average with the weights obtained.

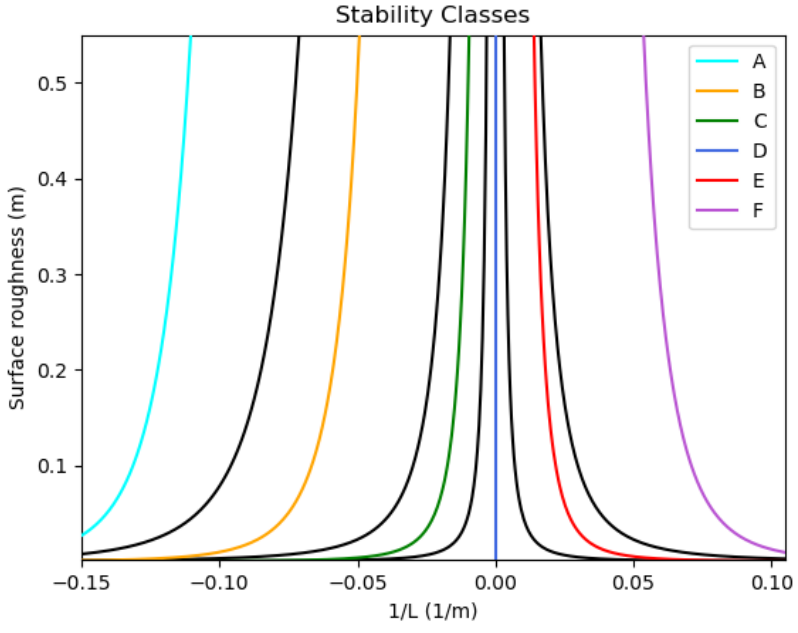

Figure 1. This figure shows the A, B, C, D, E, and F stability classes on the z_0-$1/L$ space, with the colored lines indicating the centerlines of each of the stability classes, and the black lines indicating the "border" between each of the stability classes. The axes are linear, and the units are in meters for surface roughness (y-axis) and m^{-1} for $1/L$ (x-axis).

2.2.2 Locating the Source

To further improve the emission estimates, a systematic, algorithmic approach was used to adjust the source location, nudging the source location after the initial inversion process to optimize the agreement between observed and modeled concentrations. The source location was translated along (parallel to) the transect path (i.e., the line of travel of the mobile measurement platform). If the autocorrelation between the observed and modeled concentrations was sufficiently high, meaning that there is good agreement between the modeled plume and the observation up to some translation, and if the skewness in the transects

https://doi.org/10.5194/egusphere-2025-5086
Preprint. Discussion started: 26 January 2026

were sufficiently close to each other (meaning that the model and the observation share a similar "shape"), then the source location was translated by matching the peaks in the observed and modeled concentration profiles. Kurtosis (or other moments of the distribution) was not examined in this analysis. Autocorrelation values of 0.66 to 0.955 were chosen as the cutoffs for this algorithm, and similarly, a requirement that the difference in skewness be less than 2 was also added. These values were chosen after running the model for various transects of varying quality and noise-level.

2.3 Test Sites

The methodology discussed above was tested across several diverse sites to evaluate the performance and robustness of the model/inversion setup. The sites included both natural and largely flat environments as well as more industrialized areas, both with varying levels of CH_4 emissions. The first tests were done with data collected from the Sarnia region in Southern Ontario, Canada. Controlled release campaigns were conducted in this area, near 4120 Oil Heritage Road, Petrolia, Ontario (henceforth referred to simply as the "Petrolia" site in this study), which allowed for testing of the model under known emission conditions, helping to calibrate the system and evaluate its performance in a more controlled setting. Controlled release runs were carried out on November 7th and 9th of 2023. A measurement from the same area as where the controlled release took place, but not during the experiment (July 27th, 2022) was also examined. Just south of Petrolia, other (not controlled release) measurements were also made. These measurements were collected near 161 Bickford Line, Courtright, Ontario (and labeled "Courtright" in this study). These were conducted on October 31st and November 8th of 2023. These transects came from one facility complex, but likely came from different sources within the facility. In addition to the controlled release experiments in 2023, a second controlled release campaign was conducted in May 2025 at the same location in Petrolia. In this field campaign, multiple transects of the same plume were measured by going back and forth on the same road in succession. These transects were then averaged, by overlaying the measurements on top of each other and then smoothing them by applying a Gaussian filter. This approach was tested in this campaign in an effort to minimize the effects of wind meandering and shifting. These experiments were carried out from May 16 to May 18, 2025.

Additional testing was conducted at several sites in Quebec, including an oil refinery (Energie Valero oil refinery in Lévis, Quebec, labeled "Quebec City Valero" in this study) and a recycling center (Hêtrière Ecocentre located in the District of Sainte-Foy–Sillery–Cap-Rouge, labeled "Quebec City Hêtrière" in this study) in Quebec City, and a recycling plant near Trois-Rivières (Enercycle headquarters in Saint-Étienne-des-Grès, Quebec, labeled "Trois-Rivières" in this study for simplicity). These sites were chosen for their diversity in emission sources, including CH_4 from industrial (oil & gas) processes and microbial processes (waste management). These measurements were made on November 19th, 20th, and 22nd of 2024. By testing the model at multiple sites, the study ensured that the methodology was generalizable and could be applied to a wide range of emission scenarios, providing reliable estimates of methane emissions across different sectors.

https://doi.org/10.5194/egusphere-2025-5086
Preprint. Discussion started: 26 January 2026

3 Results and Discussion

3.1 Effects of Stability Classes

The model with the posterior (after the inversion scheme) emissions generally showed similar results with the two nearest stability classes, and after blending, the statistics (e.g., correlation) were roughly the weighted averages of the two classes, and slightly better in some cases (e.g., Petrolia #4, where R^2 went from 0.94 and 0.84 to 0.96 after blending). Table 1 shows the blended classes and the respective performances. The results shown here were taken from the model runs after the source translation, which is discussed in Section 3.2. The resulting blended runs will have emission estimates that are the weighted averages of the two stability classes, and as evident in Figure 2, these tended to be more in line with measurements.

The algorithm was stable under extreme cases; for example, the Petrolia transect #5 was run with stability class F alone, as was the Quebec City Valero run (see Table 1 and Figure 3). Petrolia #4 was run blending stability classes E and F, and the inversion converged to give physical and meaningful emission estimates with a reasonably high R^2 (as noted above, this was also a case in which the blended runs resulted in slightly better correlation). In fact, it is worth noting that this stability blending methodology is stable and performs as expected regardless of which stability classes are blended (or not blended); nearly all stability classes were examined; indeed, B, C, D, E, and F classes were seen across the runs in this study (see Table 1).

However, this approach is not without problems. This approach to estimating the stability class is very sensitive to the surface roughness parameter (z_0) when $z_0 <\sim 0.1$ (see Figure 1, and note the low, nearly-flat slopes of the curves), which was often the case in Petrolia and Courtright (e.g., z_0 was roughly 0.06 in Petrolia). z_0, which in this study was taken from the HRRR reanalysis dataset, may in some cases be outdated or too coarse in resolution, or both; because the methodology discussed in this study assumes z_0 to be well-known, this can sometimes result in strange stability classes. However, without highly specialized equipment (e.g., Trepekli and Friborg, 2021, which used a LiDAR-equipped drone), making empirical measurements of z_0 can be challenging, and thus the value was taken from existing reanalysis datasets. Conversely, when $z_0 >\sim 0.2$, the stability class becomes extremely sensitive to the Obukhov length (or rather $1/L$), necessitating good estimates of L. On a similar note, a dedicated setup to measure Obukhov length (or rather the parameters needed to derive L) may result in improvements to this methodology, although this is also challenging to accomplish in a mobile setup (Araújo da Silva et al., 2022).

3.2 Emission Estimates and Source Location

The source translation algorithm generally resulted in higher correlation, lower RMSE, and higher emission estimates. The results are summarized in Table 2. The results of controlled release experiments, in which known quantities of CH_4 were released from known locations, showed particularly promising results; the algorithm in all cases found, within ∼50 meters, the correct source locations. Here, the a priori source location taken to be several hundred meters north of the actual sources. Additionally, in one of the transects (Petrolia #4), the algorithm was able to find a completely different source: a farm stable located about 1200 meters away (see Figure 4). The transect plots for this run, along with birds-eye view of the plume, are shown in Figure 5. It is also evident that this is a completely different source by looking at the estimated emission rate, estimated to be 880 ± 420 kg/d, which is roughly an order of magnitude less than the other controlled release studies (see Table 2).

https://doi.org/10.5194/egusphere-2025-5086
Preprint. Discussion started: 26 January 2026

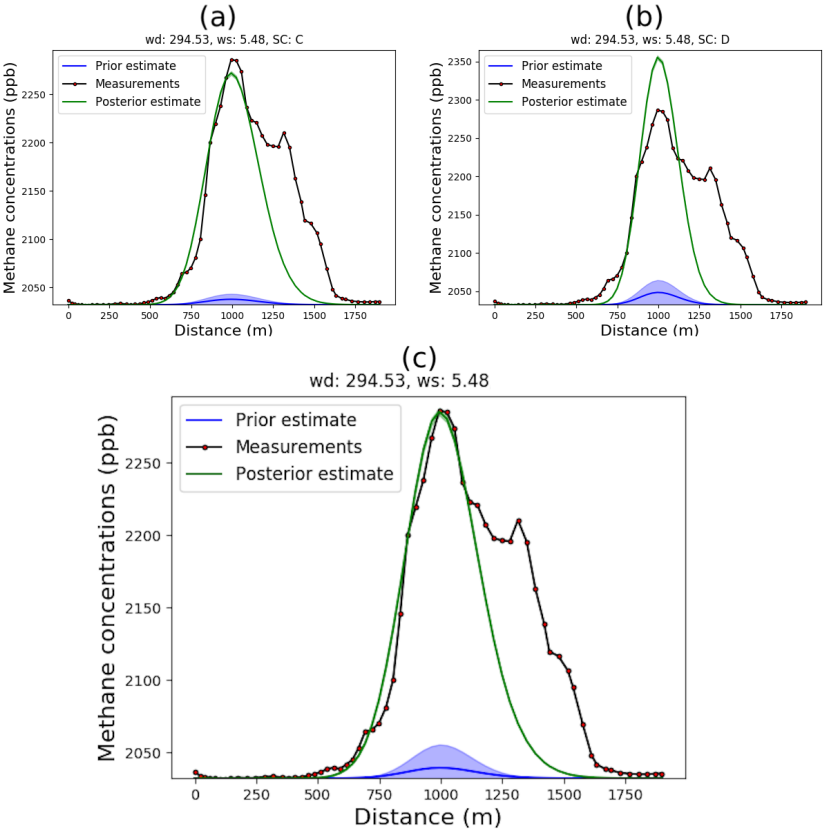

Figure 2. Transect plots showing the measurements, model prior and model posterior for Petrolia # 2, for (a) stability class C, (b) stability class D, and (c) blended. All units are in parts per billion (ppb) and meters (m).

For Petrolia #1 and #2 (controlled release experiments conducted in 2023), the actual emission rates are available for comparison; For Petrolia #2, our inversion estimate was 3380 $\pm$ 1620 kg/day while the actual rate was 3567 kg/day, and for Petrolia #1, we estimated 2770 $\pm$ 1330 kg/day, while the actual rate was 1991 kg/day. The source locating algorithm performed well and drastically improved Petrolia #2 results, but led to a further overestimation for Petrolia #1. This may be due to the uncertainty in the source location in the direction perpendicular to the transect; This is supported by the fact that the overestimation was present before the source translation took place. Furthermore, the Petrolia #2 correlation improved significantly with the source location algorithm (see Table 2), also indicating that the discrepancy in emission rates is likely not due to the uncertainty of the source location in the direction parallel to the transect.

The algorithm was also stable with "real" observational data (not from controlled release experiments). The transects from Petrolia (# 4 and #5), Quebec City, Trois-Rivières, and Courtright all show better correlation and errors after optimizing for the source location (see Table 2). The two transects from Trois-Rivières appeared to have at least two sources, two of which were fairly close to each other and well mixed by the time the plume reached the road. There also appeared to be another,

https://doi.org/10.5194/egusphere-2025-5086
Preprint. Discussion started: 26 January 2026

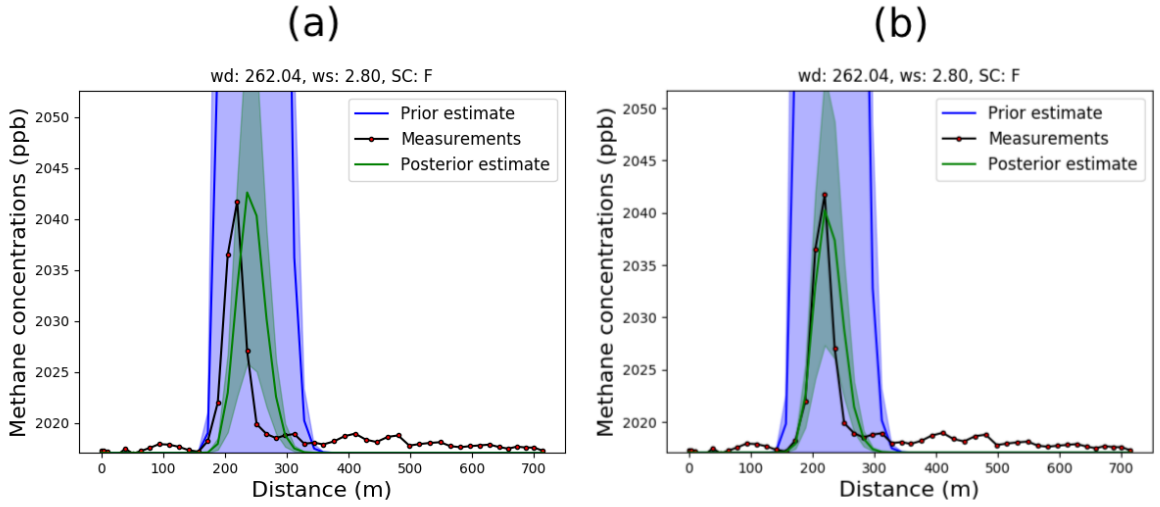

Figure 3. Transect plots showing the measurements, model prior and model posterior for the Quebec City Valero, for (a) original source location, and (b) optimized source location. All units are in parts per billion (ppb) and meters (m).

smaller source southeast of the main source; an attempt was made to evaluate the smaller signal, and indeed the source locating algorithm was able to "find" it once the a priori was nudged over, but the plume was too small and perturbed (not Gaussian in shape) to do a meaningful inversion. While the emissions from the second smaller plume could not be quantified, this does demonstrate the algorithm's ability to handle multiple sources if they are sufficiently separated (i.e., not well mixed as to form a single, larger, Gaussian-shaped plume). Note that, as mentioned in Section 2.3, transects from Courtright (#1 $\sim$ #5) likely came from different sources (within the same facility complex), and thus the emissions are not expected to agree with each other. Of the controlled release experiments, both Petrolia #1 and #2 the estimated emission rates remained the same or increased (this excludes Petrolia #4 as this was likely a completely different source, as discussed above), which is in line with the findings by Ars et al. (2017). It should be noted here that Petrolia #3 transect was on highly non-Gauissian. The method works regardless of the size of the signal; the enhancement seen in the Valero plant transect from Quebec City is very small in comparison with other sites, but the optimized run shows large improvements in both the fit and RMSE (see Figure 3 and Table 2). Furthermore, in all cases, the algorithm returned meaningful and physical results. Even without constraints or limitations on how far the source could be translated, the resulting optimized location was within the emitting facility grounds.

However, the limitation of this approach is in the second degree of freedom; it is not possible to determine the source location in the direction perpendicular to the transect path. Because the transected plume shape is the same whether the source is farther away and emitting less, or closer but emitting more, it is not possible to determine this from the transect alone. The problem caused by this invariance can be ameliorated by taking a transect from both sides, if the wind conditions and roads permit such measurements (the wind will need to be blowing in an appropriate direction, and there must be roads to make measurements). By iterating this algorithm from one side to another alternately, a better estimate on the true source location

https://doi.org/10.5194/egusphere-2025-5086
Preprint. Discussion started: 26 January 2026

Transect	Primary stability class	Secondary stability class	Primary class		Secondary class		Blended class	
			R^2	RMSE	R^2	RMSE	R^2	RMSE
Petrolia-1	C (54 %)	D (46 %)	0.92	22.4	0.94	11.2	0.94	15.8
Petrolia-2	C (84 %)	D (16 %)	0.79	41.5	0.72	52.4	0.78	42.4
Petrolia-3	B (57 %)	C (43 %)	0.86	386	0.74	580	0.82	455
[1]Petrolia-4	E (89 %)	F (11 %)	0.94	8.63	0.84	19.9	0.96	9.52
[2]Petrolia-5	F (100 %)	N/A	0.82	8.3	N/A	N/A	N/A	N/A
Quebec City Valero	F (100 %)	N/A	0.81	2.22	N/A	N/A	N/A	N/A
Quebec City Hêtrière	C (66 %)	D (34 %)	0.80	72.3	0.86	60.5	0.83	65.8
Trois-Rivières-1	C (56 %)	D (44 %)	0.85	387	0.84	440	0.85	392
Trois-Rivières-2	C (56 %)	D (44 %)	0.68	165	0.78	146	0.74	153
Courtright-1	D (59 %)	C (41 %)	0.88	67	0.86	61	0.88	60
Courtright-2	D (59 %)	C (41 %)	0.80	43	0.79	43	0.80	41
Courtright-3	C (75 %)	D (25 %)	0.87	72	0.92	44	0.89	63
Courtright-4	C (75 %)	D (25 %)	0.95	14	0.95	18	0.96	13
Courtright-5	C (75 %)	D (25 %)	0.78	2.1	0.83	1.6	0.80	1.9

Table 1. Stability classes for each of the transects and their statistics. These results are from the source-location optimized run (see Section 3.2).

[1]This observation was made during the controlled release experiment, but was likely not part of it (see Section 3.2 for more discussion).

[2]This was measured at the same location as the controlled release experiments, but was measured the previous year and not part of the controlled release campaign..

[3]These runs were from averaged transects (see Section 2.3 for more details on the averaging methodology).

may be obtained in a converging "spiraling stairwell". In practice, such conditions (wind and road) are difficult to come by, meaning that in most cases the source must be manually identified given the constraint imposed by this algorithm. Without appropriate observational data, the algorithm can still improve emission estimates *given a rough knowledge* of the source location, as shown in this study. However, for this algorithm to triangulate the source from both dimensions, observations should be carefully planned, ensuring that routes on both sides of the source are available, and all planned with wind forecast data in mind.

3.3 Averaged Plumes

For controlled release experiments carried out in 2025, transects were averaged by overlaying the measurements on top of each other, and then smoothing them by applying a Gaussian filter. This approach was tested in this campaign in an effort to minimize the effects of wind meandering and shifting. The averaging method worked well in smoothing out the noisy data, returning a more "Gaussian-like" transect even when individual transects were not (due to e.g., plume meandering. This method

https://doi.org/10.5194/egusphere-2025-5086
Preprint. Discussion started: 26 January 2026

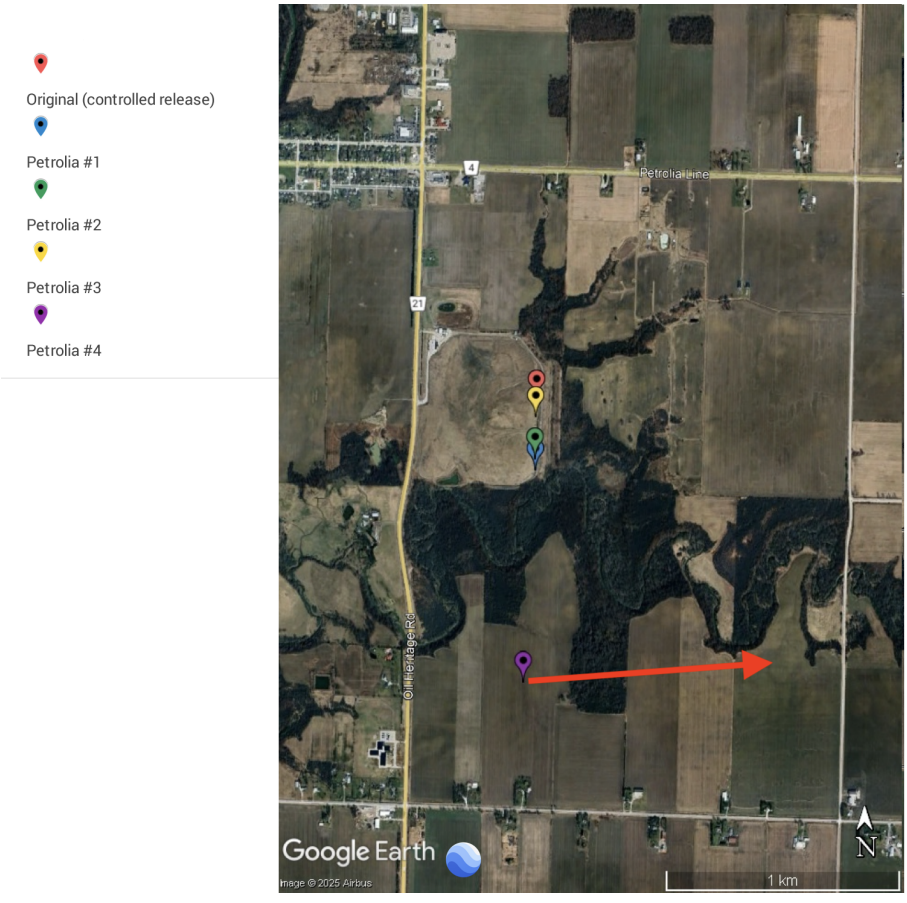

Figure 4. Satellite view of the a priori source location for the controlled release experiments at Petrolia. The bottom (southern-most) indicator optimized location for Petrolia # 4 transect) is likely from a farm to the left (west). The wind direction for this run is indicated with a red arrow by the indicator. Imagery taken from Google Earth, © Airbus, 2025.

also worked in reducing the effects of measurement delay, where measurements are slightly delayed because the air has to travel through the inlet tubing (while most of the delay is corrected during data processing, the averaging methodology aided in further improving the residual uncertainty of the delay).

The comparison between the actual reported emission rates and the model estimated emission rates (utilizing all of the methodologies discussed in this study) are shown in Figure 6. The estimated emission rates of both the source-location optimized and original (i.e., the location was simply taken to be roughly the center of the site) showed good agreement, with Pearson correlation (R) of 0.83 and 0.81, respectively. We noted an outlier point on the far right, where the model failed to accurately estimate the emission rate from a very high-emission test (10,000+ kg/day), and the statistical analysis was done without this point (it is included in the plot, however). It is worth noting that correlation remained largely unaffected by the removal of this outlier (R was 0.78 with this outlier). The estimated emissions (with uncertainty) are all within the one-to-one line

https://doi.org/10.5194/egusphere-2025-5086
Preprint. Discussion started: 26 January 2026

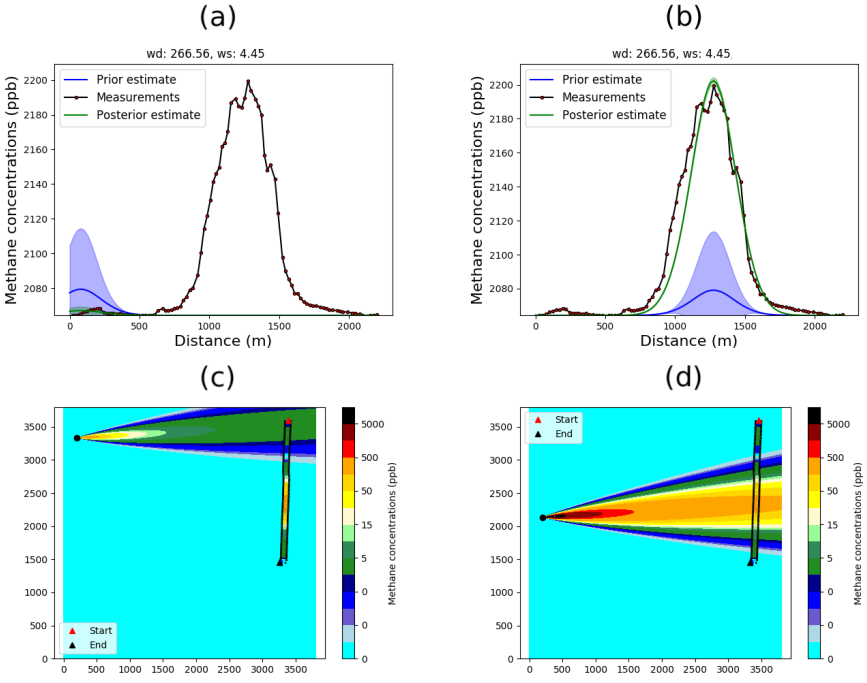

Figure 5. Transect plots showing the measurements, model prior and model posterior for the Petrolia #4, for (a) original source location, and (b) optimized source location, and the birds-eye plots showing the modeled plume and the observations for (c) original source location, and (d) optimized source location. All units are in parts per billion (ppb) and meters (m) (for (a) and (b)).

(aside from the outlier mentioned above), showing that the inversion model is able to successfully estimate the emission rates. The slope of the lines of best fit indicate overestimation; the slope was 1.27 ± 0.32 and 1.19 ± 0.32 for the source-optimized and original estimates, respectively. Interestingly, unlike the results from the individual transects, running the source-algorithm did not strictly increase emissions estimates (this is also evident from the slopes on the lines of best fit). This is likely because the averaging of the transects masked the effects of meandering and shifting winds on the plume, as well as the uncertainty associated with the source location.

4 Conclusions

The use of Gaussian dispersion model inversion allows for a simple, computationally efficient, yet robust estimations of emissions of GHGs such as CH_4 at the facility scale. In this study, we proposed and tested novel improvements to the existing Gaussian dispersion model framework, by blending, with appropriate weights, the nearest two stability classes to get a more continuous and less discretized model of atmospheric conditions, and imposing a simple algorithm to translate the source location along the direction of the transect to improve the fit. A Gaussian dispersion model in the Polyphemus suite was used in

https://doi.org/10.5194/egusphere-2025-5086
Preprint. Discussion started: 26 January 2026

Transect	Before			After			Distance/direction of translation
	R^2	RMSE	Emission rate	R^2	RMSE	Emission rate	
Petrolia-1	0.40	34.3	2270 ± 1090	0.94	15.8	2770 ± 1330	296 m, south
Petrolia-2	0.01	95.3	1640 ± 790	0.78	42.4	3380 ± 1620	246 m, south
Petrolia-3	0.66	840	19070 ± 9150	0.82	455	14213 ± 6820	70 m, south
[1]Petrolia-4	0.08	51.9	20 ± 10	0.96	9.52	880 ± 420	1200m, south
[2]Petrolia-5	0.78	9.2	17 ± 8	0.82	8.3	18 ± 9	8.2 m, east
Quebec City Valero	0.32	4.75	1.9 ± 0.9	0.81	2.22	1.7 ± 0.8	16 m, northwest
Quebec City Hêtrière	0.04	160	340 ± 160	0.83	65.8	790 ± 380	83 m, north
Trois-Rivières-1	0.34	933	11920 ± 5720	0.85	392	10370 ± 4980	82 m, southwest
Trois-Rivières-2	0.58	194	7000 ± 3360	0.74	153	6670 ± 3200	58 m, northwest
Courtright-1	0.04	201	310 ± 150	0.88	59.7	730 ± 350	137 m, east
Courtright-2	0.03	102	148 ± 71	0.80	41.1	330 ± 160	60 m. west
Courtright-3	0.17	205	440 ± 210	0.89	63.2	1030 ± 490	184 m, south
Courtright-4	0.02	68.9	180 ± 86	0.96	12.8	400 ± 190	123 m, south
Courtright-5	0.19	6.70	53 ± 25	0.80	1.88	32 ± 15	226 m, south

Table 2. Correlation (R^2), RMSE, and the posterior emission rates (in kg/day) for before and after the source location optimization for each of the transect runs. The distance (in meters) and the general direction of the source translation is also tabulated. The results listed are from runs with "blended" stability class (see Section 2.2.1).

[1]This observation was made during the controlled release experiment, but was likely not part of it (see Section 3.2 for more discussion).

[2]This was measured at the same location as the controlled release experiments, but was measured the previous year and not part of the controlled release campaign.

this study, with meteorological data from HRRRv4. This was compared against observational CH_4 data from mobile measurements, where real-time data is collected from a vehicle-mounted sensor setup. A Bayesian inversion was performed to estimate emissions from the source. The stability class were blended with weights (of the weighted averages) derived by calculating the Obukhov length examining its value along with the surface roughness (from HRRR data). The source location, which in many cases is not exactly known, was allowed to vary along the direction of the transect, and an algorithm that examines correlation, plume maximal location, autocorrelation (and lag), and skewness was utilized to determine if translating the source was needed, and by how much.

The results show that the model improves and gives better fits after translating the source in all scenarios examined in this study. Correlation increased and RMSE decreased in all instances, and the algorithm in one instance was able to "find" a new source over a kilometer away. While improvements in R^2 ranged from minor (0.78 to 0.82, seen in Petrolia #5) to major (e.g., 0.02 to 0.96 seen in Courtright #4), the former was the exception; most improvements were large and significant. The shape of the transect also qualitatively improved, and the algorithm was stable under all of the scenarios examined in this study. This

https://doi.org/10.5194/egusphere-2025-5086
Preprint. Discussion started: 26 January 2026

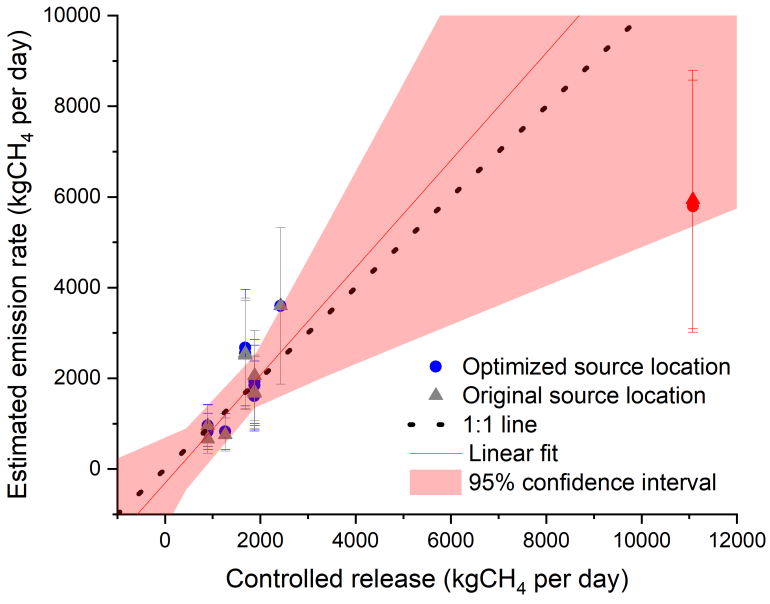

Figure 6. Scatterplot comparing the actual reported emission rates and the model estimated emission rates, in kg/day. Blue points and red line indicate the estimates with the source location optimization algorithm, while the grey points indicate the estimates prior to the source location optimization. The dashed black line indicates the line of unity (one-to-one). Red shaded area indicates the 95% confidence interval.

approach showed improvements both with controlled release data and "real" observational data. The model, with the stability classes blended, showed slight improvements in a few instances, but generally showed results that were the weighted averages of the two blended classes, which was expected. This includes the emission rate estimates, and in many cases this tended to be more in line with observations. In this study, all stability classes except for A were observed (from B to F), and the method worked without issues, converging to give physical and meaningful emissions estimates.

This approach relies on, and is very sensitive to surface roughness (when $z_0 <\sim 0.1$) and Obukhov length (when $z_0 >\sim 0.2$), and the value of z_0 that was obtained from HRRR may be outdated in some areas, possibly leading to misclassifications. Empirically measuring surface roughness was outside the scope of this study, although improvements in this could lead to significantly better, more robust stability classifications (and weights associated with the blending). Similarly, making empirical measurements of Obukhov length could also be another future work. Indeed, one of our future work includes measuring Obukhov length using a stationary (i.e., not onboard the car), high-frequency anemometer to assess, compare with, and better understand the derived value from HRRR data; this approach requires the anemometer to be setup before driving through the plume to measure transects, meaning it is ill-suited for campaigns where multiple sites are visited throughout the day, and realistically can only be used for case studies that focus on estimating emissions from a particular source. Other possible future work and

https://doi.org/10.5194/egusphere-2025-5086
Preprint. Discussion started: 26 January 2026

improvements to the approach discussed here include obtaining more transects to improve the source locating algorithm; the method discussed here does indeed improve the estimates on source location parallel to the transect, but is not able to determine how far away the source is, from the road where the measurements are made. This could be remedied by having measurements from sides that are orthogonal to each other (e.g., west side and north side) allowing the algorithm to refine, and converge onto, the source location in a "spiraling stairwell" like manner. This was not tested in this study due to limited data, which in many cases was due to uncontrollable factors such as wind direction; a controlled release study conducted over a longer period to ensure favorable wind conditions will allow this methodology to be tested on both axes. Indeed, there are plans to conduct future experiments to provide data to test the spiraling stairwell approach. The latest controlled release campaign involved testing a method in which multiple transects from the same road were averaged and smoothed before running the inverse modeling. This methodology worked well in smoothing out the noisy data, as well as reducing the effects of measurement delay, where measurements are slightly delayed because the air has to travel through the inlet tubing. Comparing with model estimated emission rates and the actual reported emission rates showed decent agreement (Pearson correlation of 0.83), although the model had challenges accurately estimating the emission rate from a very high-emission test (10,000+ kg/day).

Overall, the study describes and tests novel improvements to the Gaussian dispersion model, showcasing that the methods presented, while they have limitations - such as the inability to fully triangulate the source and the sensitivity to surface roughness - do indeed improve the model and inversion, giving meaningful results across a variety of real-world scenarios.

Code availability. The source code used for blending stability classes is publicly available here: Doi: 10.5281/zenodo.18190453 as well as on the PyPI Python packages repository and Github (e.g., https://test.pypi.org/project/blendie/), or from authors upon request. The Polyphemus suite, including the Gaussian dispersion model used in this study, is available for download at Doi: 10.5281/zenodo.10067062, with documentation and user guide available at https://cerea.enpc.fr/polyphemus/ (last accessed April, 2025). The code used for the methane inversion can be found at Doi: 10.5281/zenodo.18249816, details of which are described in Ars et al. (2017).

Data availability. Data used in this study are available at Doi: 10.18164/2264d3b1-761e-4521-9ebb-0b8124d1dab4 (Yamanouchi, 2025). The meteorological data extracted from HRRRv4 used in this study are available at Doi: 10.5281/zenodo.18319805. For more information on HRRR, see https://rapidrefresh.noaa.gov/hrrr/ and Doi: 10.1175/WAF-D-21-0151.1.

Author contributions. The model improvements were made by SY with valuable input from FV. FV, SA, LG, MF, and SY participated in data collection, and SY, FV, SA, and KR aided with data processing. SY wrote the manuscript with input from all authors.

Competing interests. There are no competing interests to declare.

https://doi.org/10.5194/egusphere-2025-5086
Preprint. Discussion started: 26 January 2026

Acknowledgements. This work was funded by Environment and Climate Change Canada, and Natural Resources Canada's Program on Energy Research and Development. Authors thank Yelva Roustan (CEREA, Marne-la-Vallee, France) for valuable, detailed, and technical input that helped improve this study. Controlled release testing was performed at the SIMFLEX site (https://fluxlab.ca/simflex/), which was established with support from the Environmental Research & Education Foundation (EREF), and the Natural Sciences and Engineering Research Council of Canada (NSERC). We want to specifically thank Prof. Dave Risk and the FluxLab team from St. Francis Xavier University.

https://doi.org/10.5194/egusphere-2025-5086
Preprint. Discussion started: 26 January 2026

References

Alexe, M., Bergamaschi, P., Segers, A., Detmers, R., Butz, A., Hasekamp, O., Guerlet, S., Parker, R., Boesch, H., Frankenberg, C., Scheepmaker, R. A., Dlugokencky, E., Sweeney, C., Wofsy, S. C., and Kort, E. A.: Inverse modelling of CH_4 emissions for 2010–2011 using different satellite retrieval products from GOSAT and SCIAMACHY, Atmospheric Chemistry and Physics, 15, 113–133, Doi: 10.5194/acp-15-113-2015, 2015.

Araújo da Silva, M. P., Rocadenbosch, F., Farré-Guarné, J., Salcedo-Bosch, A., González-Marco, D., and Peña, A.: Assessing Obukhov Length and Friction Velocity from Floating Lidar Observations: A Data Screening and Sensitivity Computation Approach, Remote Sensing, 14, Doi: 10.3390/rs14061394, 2022.

Ars, S., Broquet, G., Yver Kwok, C., Roustan, Y., Wu, L., Arzoumanian, E., and Bousquet, P.: Statistical atmospheric inversion of local gas emissions by coupling the tracer release technique and local-scale transport modelling: a test case with controlled methane emissions, Atmospheric Measurement Techniques, 10, 5017–5037, Doi: 10.5194/amt-10-5017-2017, 2017.

Ars, S., Vogel, F., Arrowsmith, C., Heerah, S., Knuckey, E., Lavoie, J., Lee, C., Pak, N. M., Phillips, J. L., and Wunch, D.: Investigation of the Spatial Distribution of Methane Sources in the Greater Toronto Area Using Mobile Gas Monitoring Systems, Environmental Science & Technology, 54, 15 671–15 679, Doi: 10.1021/acs.est.0c05386, 2020.

Bergamaschi, P., Karstens, U., Manning, A. J., Saunois, M., Tsuruta, A., Berchet, A., Vermeulen, A. T., Arnold, T., Janssens-Maenhout, G., Hammer, S., Levin, I., Schmidt, M., Ramonet, M., Lopez, M., Lavric, J., Aalto, T., Chen, H., Feist, D. G., Gerbig, C., Haszpra, L., Hermansen, O., Manca, G., Moncrieff, J., Meinhardt, F., Necki, J., Galkowski, M., O'Doherty, S., Paramonova, N., Scheeren, H. A., Steinbacher, M., and Dlugokencky, E.: Inverse modelling of European CH_4 emissions during 2006–2012 using different inverse models and reassessed atmospheric observations, Atmospheric Chemistry and Physics, 18, 901–920, Doi: 10.5194/acp-18-901-2018, 2018.

Briggs, G.: Chimney plumes in neutral and stable surroundings$_{**}$Shwartz and Tulin, Atmospheric Environment6, 19–35 (1971)., Atmospheric Environment (1967), 6, 507–510, Doi: https://doi.org/10.1016/0004-6981(72)90120-5, 1972.

Chan, E., Worthy, D. E. J., Chan, D., Ishizawa, M., Moran, M. D., Delcloo, A., and Vogel, F.: Eight-Year Estimates of Methane Emissions from Oil and Gas Operations in Western Canada Are Nearly Twice Those Reported in Inventories, Environmental Science & Technology, 54, 14 899–14 909, Doi: 10.1021/acs.est.0c04117, 2020.

Chang, J., Peng, S., Ciais, P., Saunois, M., Dangal, S. R., Herrero, M., Havlík, P., Tian, H., and Bousquet, P.: Revisiting enteric methane emissions from domestic ruminants and their δ13CCH4 source signature, Nature Communications, 10, 3420, 2019.

Christensen, J.: Emissions Gap Report 2018, UNEP DTU Partnership, 2018.

Cusworth, D. H., Bloom, A. A., Ma, S., Miller, C. E., Bowman, K., Yin, Y., Maasakkers, J. D., Zhang, Y., Scarpelli, T. R., Qu, Z., Jacob, D. J., and Worden, J. R.: A Bayesian framework for deriving sector-based methane emissions from top-down fluxes, Communications Earth & Environment, 2, 242, Doi: 10.1038/s43247-021-00312-6, 2021.

Dowell, D. C., Alexander, C. R., James, E. P., Weygandt, S. S., Benjamin, S. G., Manikin, G. S., Blake, B. T., Brown, J. M., Olson, J. B., Hu, M., Smirnova, T. G., Ladwig, T., Kenyon, J. S., Ahmadov, R., Turner, D. D., Duda, J. D., and Alcott, T. I.: The High-Resolution Rapid Refresh (HRRR): An Hourly Updating Convection-Allowing Forecast Model. Part I: Motivation and System Description, Weather and Forecasting, 37, 1371 – 1395, Doi: 10.1175/WAF-D-21-0151.1, 2022.

https://doi.org/10.5194/egusphere-2025-5086
Preprint. Discussion started: 26 January 2026

Ganesan, A. L., Manning, A. J., Grant, A., Young, D., Oram, D. E., Sturges, W. T., Moncrieff, J. B., and O'Doherty, S.: Quantifying methane and nitrous oxide emissions from the UK and Ireland using a national-scale monitoring network, Atmospheric Chemistry and Physics, 15, 6393–6406, Doi: 10.5194/acp-15-6393-2015, 2015.

Gillespie, L. D., Ars, S., Alkadri, S., Urya, S., Khoo, T., Fraser, S., Vogel, F., and Wunch, D.: Estimating methane emissions from the waste sector in Southern Ontario using atmospheric measurements, Journal of the Air & Waste Management Association, 75, 144–163, Doi: 10.1080/10962247.2024.2435340, 2025.

Golder, D.: Relations among stability parameters in the surface layer, Boundary-Layer Meteorology, 3, 47–58, 1972.

Hansen, J., Sato, M., Ruedy, R., Lacis, A., and Oinas, V.: Global warming in the twenty-first century: An alternative scenario, Proceedings of the National Academy of Sciences, 97, 9875–9880, Doi: 10.1073/pnas.170278997, 2000.

Hosseini, B. and Stockie, J. M.: Bayesian estimation of airborne fugitive emissions using a Gaussian plume model, Atmospheric Environment, 141, 122–138, Doi: https://doi.org/10.1016/j.atmosenv.2016.06.046, 2016.

IPCC: Summary for Policymakers, p. 1–30, Cambridge University Press, Doi: 10.1017/CBO9781107415324.004, 2014.

Johnson, M. R., Tyner, D. R., Conley, S., Schwietzke, S., and Zavala-Araiza, D.: Comparisons of Airborne Measurements and Inventory Estimates of Methane Emissions in the Alberta Upstream Oil and Gas Sector, Environmental Science & Technology, 51, 13 008–13 017, Doi: 10.1021/acs.est.7b03525, 2017.

MacKay, K., Lavoie, M., Bourlon, E., Atherton, E., O'Connell, E., Baillie, J., Fougère, C., and Risk, D.: Methane emissions from upstream oil and gas production in Canada are underestimated, Scientific Reports, 11, 8041, Doi: 10.1038/s41598-021-87610-3, 2021.

Mallet, V., Quélo, D., Sportisse, B., Ahmed de Biasi, M., Debry, E., Korsakissok, I., Wu, L., Roustan, Y., Sartelet, K., Tombette, M., and Foudhil, H.: Technical Note: The air quality modeling system Polyphemus, Atmospheric Chemistry and Physics, 7, 5479–5487, Doi: 10.5194/acp-7-5479-2007, 2007.

Melton, J. R., Wania, R., Hodson, E. L., Poulter, B., Ringeval, B., Spahni, R., Bohn, T., Avis, C. A., Beerling, D. J., Chen, G., Eliseev, A. V., Denisov, S. N., Hopcroft, P. O., Lettenmaier, D. P., Riley, W. J., Singarayer, J. S., Subin, Z. M., Tian, H., Zürcher, S., Brovkin, V., van Bodegom, P. M., Kleinen, T., Yu, Z. C., and Kaplan, J. O.: Present state of global wetland extent and wetland methane modelling: conclusions from a model inter-comparison project (WETCHIMP), Biogeosciences, 10, 753–788, Doi: 10.5194/bg-10-753-2013, 2013.

Miller, S. M., Wofsy, S. C., Michalak, A. M., Kort, E. A., Andrews, A. E., Biraud, S. C., Dlugokencky, E. J., Eluszkiewicz, J., Fischer, M. L., Janssens-Maenhout, G., Miller, B. R., Miller, J. B., Montzka, S. A., Nehrkorn, T., and Sweeney, C.: Anthropogenic emissions of methane in the United States, Proceedings of the National Academy of Sciences, 110, 20 018–20 022, Doi: 10.1073/pnas.1314392110, 2013.

Nisbet, E. G., Fisher, R. E., Lowry, D., France, J. L., Allen, G., Bakkaloglu, S., Broderick, T. J., Cain, M., Coleman, M., Fernandez, J., Forster, G., Griffiths, P. T., Iverach, C. P., Kelly, B. F. J., Manning, M. R., Nisbet-Jones, P. B. R., Pyle, J. A., Townsend-Small, A., al Shalaan, A., Warwick, N., and Zazzeri, G.: Methane Mitigation: Methods to Reduce Emissions, on the Path to the Paris Agreement, Reviews of Geophysics, 58, e2019RG000 675, Doi: https://doi.org/10.1029/2019RG000675, 2020.

Poulter, B., Bousquet, P., Canadell, J. G., Ciais, P., Peregon, A., Saunois, M., Arora, V. K., Beerling, D. J., Brovkin, V., Jones, C. D., Joos, F., Gedney, N., Ito, A., Kleinen, T., Koven, C. D., McDonald, K., Melton, J. R., Peng, C., Peng, S., Prigent, C., Schroeder, R., Riley, W. J., Saito, M., Spahni, R., Tian, H., Taylor, L., Viovy, N., Wilton, D., Wiltshire, A., Xu, X., Zhang, B., Zhang, Z., and Zhu, Q.: Global wetland contribution to 2000–2012 atmospheric methane growth rate dynamics, Environmental Research Letters, 12, 094 013, Doi: 10.1088/1748-9326/aa8391, 2017.

Smith, C., Nicholls, Z., Armour, K., Collins, W., Forster, P., Meinshausen, M., Palmer, M., and Watanabe, M.: The Earth's Energy Budget, Climate Feedbacks, and Climate Sensitivity Supplementary Material, https://www.ipcc.ch/, 2021.

https://doi.org/10.5194/egusphere-2025-5086
Preprint. Discussion started: 26 January 2026

Tarantola, A.: Inverse Problem Theory and Methods for Model Parameter Estimation, Society for Industrial and Applied Mathematics, Doi: 10.1137/1.9780898717921, 2005.

Trepekli, K. and Friborg, T.: Deriving Aerodynamic Roughness Length at Ultra-High Resolution in Agricultural Areas Using UAV-Borne LiDAR, Remote Sensing, 13, Doi: 10.3390/rs13173538, 2021.

Tyner, D. R. and Johnson, M. R.: Where the Methane Is—Insights from Novel Airborne LiDAR Measurements Combined with Ground Survey Data, Environmental Science & Technology, 55, 9773–9783, Doi: 10.1021/acs.est.1c01572, 2021.

Vogel, F., Ars, S., Wunch, D., Lavoie, J., Gillespie, L., Maazallahi, H., Röckmann, T., Nęcki, J., Bartyzel, J., Jagoda, P., Lowry, D., France, J., Fernandez, J., Bakkaloglu, S., Fisher, R., Lanoiselle, M., Chen, H., Oudshoorn, M., Yver-Kwok, C., Defratyka, S., Morgui, J. A., Estruch, C., Curcoll, R., Grossi, C., Chen, J., Dietrich, F., Forstmaier, A., Denier van der Gon, H. A. C., Dellaert, S. N. C., Salo, J., Corbu, M., Iancu, S. S., Tudor, A. S., Scarlat, A. I., and Calcan, A.: Ground-Based Mobile Measurements to Track Urban Methane Emissions from Natural Gas in 12 Cities across Eight Countries, Environmental Science & Technology, 58, 2271–2281, Doi: 10.1021/acs.est.3c03160, 2024.

Yadav, V., Duren, R., Mueller, K., Verhulst, K. R., Nehrkorn, T., Kim, J., Weiss, R. F., Keeling, R., Sander, S., Fischer, M. L., Newman, S., Falk, M., Kuwayama, T., Hopkins, F., Rafiq, T., Whetstone, J., and Miller, C.: Spatio-temporally Resolved Methane Fluxes From the Los Angeles Megacity, Journal of Geophysical Research: Atmospheres, 124, 5131–5148, Doi: https://doi.org/10.1029/2018JD030062, 2019.

Yamanouchi, S.: 2023-2024 ACES Mobile Survey Data, Doi: 10.18164/2264d3b1-761e-4521-9ebb-0b8124d1dab4, 2025.

Zhang, Y., Jacob, D. J., Lu, X., Maasakkers, J. D., Scarpelli, T. R., Sheng, J.-X., Shen, L., Qu, Z., Sulprizio, M. P., Chang, J., Bloom, A. A., Ma, S., Worden, J., Parker, R. J., and Boesch, H.: Attribution of the accelerating increase in atmospheric methane during 2010–2018 by inverse analysis of GOSAT observations, Atmospheric Chemistry and Physics, 21, 3643–3666, Doi: 10.5194/acp-21-3643-2021, 2021.